Multicomponent Olivine Cathode for Lithium Rechargeable Batteries: A First-Principles Study

ARTICLE *in* CHEMISTRY OF MATERIALS · JANUARY 2010

Impact Factor: 8.35 · DOI: 10.1021/cm903138s

5 AUTHORS, INCLUDING:

Dong-Hwa Seo

Massachusetts Institute of Technology

51 PUBLICATIONS **2,255** CITATIONS

SEE PROFILE

518 *Chem. Mater.* **2010,** *22,* 518–523
DOI:10.1021/cm903138s

CHEMISTRY OF MATERIALS
Article

Multicomponent Olivine Cathode for Lithium Rechargeable Batteries: A First-Principles Study

Dong-Hwa Seo, Hyeokjo Gwon, Sung-Wook Kim, Jongsoon Kim, and Kisuk Kang*

Department of Materials Science and Engineering and KAIST Institute for Eco-Energy, KAIST 335 Gwahangno, Yuseong-gu, Daejeon 305-701, Republic of Korea

Received October 12, 2009. Revised Manuscript Received December 1, 2009

The in-depth study of the multicomponent effect on the structural and electrochemical properties of olivine cathodes is conducted using state-of-the-art first-principles calculations. The distribution of multiple transition metals in olivine structure alters local crystal structure and electronic structure, affecting its kinetic and thermodynamic properties. We find that local structure change, such as the reduced Jahn−Teller effect of Mn, significantly enhances both Li mobility and electron (polaron) conductivity when the redox Mn element neighbors Fe or Co. The unexpected one-phase Li insertion/extraction reaction of the multicomponent olivine cathode is explained with respect to the multiple interactions of M/Li or M/vacancy (M = transition metals). The redox potential of each transition metal also could shift as a result of charge redistribution and the relative energy change from the multiple M/Li interactions. Implications of multicomponent olivine as a useful strategy for tailoring the electrochemical properties of olivine compounds are discussed for designing better-performing Li rechargeable batteries.

1. Introduction

Electrochemical energy storage devices are attracting tremendous interest due to the recent growing importance of sustainability and environmental concerns.[1,2] The lithium rechargeable battery is one of the most advanced energy storage systems and serves as a major power source for various small electronic devices. With the growing interest in power sources for large applications such as the HEV (hybrid electric vehicle) or PHEV (plug-in hybrid electric vehicle), lithium rechargeable batteries are finding new opportunities in this emerging area. Intensive research efforts are focused on developing suitable electrode material, the key component of Li rechargeable batteries, for these applications. The electrode material for lithium rechargeable batteries for use in HEVs and PHEVs requires highly stability, high power, high energy, and low cost.[3−7] The lithium transition metal phosphate $LiMPO_4$ (where M = Mn, Fe, Co, Ni) with an olivine structure has been highlighted as one of the most promising cathode materials owing to its advantages over current cathode material in that it is remarkably stable even in harsh operating conditions, nontoxic, and potentially inexpensive.[8−16] Recently it has been reported that the rate capability and cyclability of $LiFePO_4$ have been achieved at an almost commercial level.[17,18] However, the intrinsic low energy density of $LiFePO_4$ due to its relatively low equilibrium potential (~3.4 V) is a major hurdle to its application. To counterbalance such an effect, substitution of other metals for Fe in the olivine framework has been explored by many researchers.[14,19,20] In particular, Mn-based olivine compound has attracted great attention owing to its redox potential Mn^{3+}/Mn^{2+} of

*To whom correspondence should be addressed. E-mail: matlgen1@kaist.ac.kr. Tel.: +82-42-350-3341. Fax: +82-42-350-3310.

(1) Winter, M.; Brodd, R. J. *Chem. Rev.* **2004**, *104*(10), 4245–4270.
(2) Armand, M.; Tarascon, J. M. *Nature* **2008**, *451*(7179), 652–657.
(3) Kang, K.; Meng, Y. S.; Breger, J.; Grey, C. P.; Ceder, G. *Science* **2006**, *311*(5763), 977–980.
(4) Nishimura, S.; Kobayashi, G.; Ohoyama, K.; Kanno, R.; Yashima, M.; Yamada, A. *Nat. Mater.* **2008**, *7*(9), 707–711.
(5) Gibot, P.; Casas-Cabanas, M.; Laffont, L.; Levasseur, S.; Carlach, P.; Hamelet, S.; Tarascon, J. M.; Masquelier, C. *Nat. Mater.* **2008**, *7*(9), 741–747.
(6) *FreedomCar Battery Test Manual For Power-Assist Hybrid Electric Vehicles, DOE/ID-11069*; US Department of Energy: Idaho, 2003.
(7) Kim, S.-W.; Han, T. H.; Kim, J.; Gwon, H.; Moon, H.-S.; Kang, S.-W.; Kim, S. O.; Kang, K. *ACS Nano* **2009**, *3*(5), 1085–1090.
(8) Delacourt, C.; Poizot, P.; Morcrette, M.; Tarascon, J. M.; Masquelier, C. *Chem. Mater.* **2004**, *16*(1), 93–99.
(9) Padhi, A. K.; Nanjundaswamy, K. S.; Goodenough, J. B. *J. Electrochem. Soc.* **1997**, *144*(4), 1188–1194.
(10) Huang, H.; Yin, S. C.; Nazar, L. F. *Electrochem. Solid State Lett.* **2001**, *4*(10), A170–A172.
(11) Herle, P. S.; Ellis, B.; Coombs, N.; Nazar, L. F. *Nat. Mater.* **2004**, *3* (3), 147–152.
(12) Zhou, F.; Cococcioni, M.; Kang, K.; Ceder, G. *Electrochem. Commun.* **2004**, *6*(11), 1144–1148.
(13) Chung, S. Y.; Bloking, J. T.; Chiang, Y. M. *Nat. Mater.* **2002**, *1*(2), 123–128.
(14) Yamada, A.; Takei, Y.; Koizumi, H.; Sonoyama, N.; Kanno, R.; Itoh, K.; Yonemura, M.; Kamiyama, T. *Chem. Mater.* **2006**, *18*(3), 804–813.
(15) Delacourt, C.; Laffont, L.; Bouchet, R.; Wurm, C.; Leriche, J. B.; Morcrette, M.; Tarascon, J. M.; Masquelier, C. *J. Electrochem. Soc.* **2005**, *152*, A913–A921.
(16) Kim, S.-W.; Kim, J.; Gwon, H.; Kang, K. *J. Electrochem. Soc.* **2009**, *156*(8), A635–A638.
(17) A123 Systems. http://www.a123systems.com (accessed December **2009**).
(18) Hydro Quebec. http://www.hydroquebec.com (accessed December **2009**).
(19) Yamada, A.; Kudo, Y.; Liu, K. Y. *J. Electrochem. Soc.* **2001**, *148* (7), A747–A754.
(20) Malik, R.; Zhou, F.; Ceder, G. *Phys. Rev. B* **2009**, *79*(21), 214201–7.

 Published on Web 12/23/2009

about 4.1 V,[8,13,14] although numerous limitations in electrochemical activity, mainly due to the sluggish kinetics, are still unresolved.[19,21−23] Recently, multicomponent olivine compounds such as binary, ternary, or even quaternary systems containing Mn, Fe, Co, Mg, and Ni have been investigated for their potential use as cathode materials.[24−31] Interesting new phenomena involving multicomponent olivine systems are being discovered, such as the shift of transition metal redox potential,[9,14,20,27,30] mixed two-phase and one-phase Li de/intercalation reactions at different lithium compositions,[20,32] conversion from two-phase to one-phase Li de/intercalation reactions with multicomponent doping,[27] and different rate behavior.[31] Experimental and theoretical studies have been successfully performed on some of these phenomena in binary olivine systems such as $Li_x(Fe_{1-y}Mn_y)PO_4$.[14,19,20,30,32,33] However, in-depth theoretical understanding about the effects of ternary components on olivine cathode materials and what causes these differences has not been clearly achieved yet.

In this work, we report the effect of the substitution of multiple transition metals on the structural and electrochemical properties of olivine compounds using first-principles calculations for a model system of $LiMn_{1/3}Fe_{1/3}Co_{1/3}PO_4$. We find that Li mobility, electron (polaron) conductivity, Jahn−Teller effect of Mn, transition metal redox potential, and Li de/intercalation reaction process can be significantly altered by the presence of multiple transition metals. We also discuss the detailed mechanisms and effects on the electrochemical performance of olivine cathode material.

2. Computational Details

All energies were calculated with the spin-polarized generalized gradient approximation (GGA) using the Perdew−Burke−Ernzerhof exchange-correlation parametrization[34] to density functional theory (DFT), using a plane-wave basis set and the projector-augmented wave (PAW) method, as implemented in the Vienna ab initio simulation package (VASP).[35] PAW potentials have been widely used for battery materials and have shown good predictive capability.[3,36−40] All calculations were performed in supercells ($a \times 2b \times 3c$) of 24 formula units of $Li_xMn_{1/3}Fe_{1/3}Co_{1/3}PO_4$ at $x = 1$, $x = {}^2/_3$, $x = {}^1/_3$, and $x = 0$ and Li_xMPO_4 (M = Mn, Fe, Co) at $x = 1$ and $x = 0$. For $Li_xMn_{1/3}Fe_{1/3}Co_{1/3}PO_4$, three kinds of transition metal ions are well mixed, as shown in Figure 1. A plane-wave basis with a kinetic energy cutoff of 500 eV was used, and appropriate k-point meshes were chosen to ensure that the total energies are converged within 2 meV per formula unit. All structures were fully relaxed with antiferromagnetic orderings.

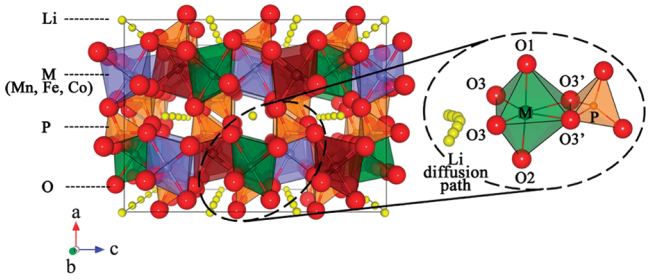

Figure 1. The structure of $Li_xMn_{1/3}Fe_{1/3}Co_{1/3}PO_4$ and local geometry of the MO_6 octahedra in $Li_xMn_{1/3}Fe_{1/3}Co_{1/3}PO_4$.

Large errors in the electronic structure are often reported for systems with strong localization of the metal d orbitals, such as phosphate materials, when calculated with GGA or local density approximation (LDA).[37,38] This is mainly due to the strong electron correlation within the d state. The GGA + U approach,[41,42] therefore, was used to accurately calculate structural and electronic properties of transition metal olvine. We employed the rotationally invariant scheme as presented by Liechtenstein.[42] The U is the onsite coulomb term and the J is the exchange term in the GGA + U approach. The self-consistently calculated U values which are averaged with U values of the M^{2+} and M^{3+} were used (U[Mn] = 5.5 eV, U[Fe] = 5.3 eV, and U[Co] = 6.7 eV),[37] and J values of 1 eV were used for all cases.

The diffusion of Li with small polarons was investigated following the approach used in our previous study.[40] Activation barrier calculations were performed with the nudged elastic band (NEB) method[43] in supercells ($a \times 2b \times 3c$) containing 24 formula units (the primitive cell contains four formula units) and were done using ferromagnetic spin polarization.[44] The large supercell isolates the hopping atoms from their periodic images, providing an accurate answer for activation barriers. For activation barriers of migrating of Li-polaron of

(21) Maxisch, T.; Zhou, F.; Ceder, G. *Phys. Rev. B* **2006**, *73*(10), 6.
(22) Meethong, N.; Huang, H. Y. S.; Speakman, S. A.; Carter, W. C.; Chiang, Y. M. *Adv. Funct. Mater.* **2007**, *17*, 1115–1123.
(23) Delacourt, C.; Poizot, P.; Levasseur, S.; Masquelier, C. *Electrochem. Solid State Lett.* **2006**, *9*(7), A352–A355.
(24) Shanmukaraj, D.; Murugan, R. *Ionics* **2004**, *10*(1−2), 88–92.
(25) Kishore, M.; Varadaraju, U. V. *Mater. Res. Bull.* **2005**, *40*(10), 1705–1712.
(26) Kuo, H. T.; Chan, T. S.; Bagkar, N. C.; Liu, G. Q.; Liu, R. S.; Shen, C. H.; Shy, A. S.; Xing, X. K.; Chen, J. M. *J. Phys. Chem. B* **2008**, *112*(27), 8017–8023.
(27) Gwon, H.; Seo, D.-H.; Kim, S.-W.; Kim, J.; Kang, K. *Adv. Funct. Mater.* **2009**, *19*(20), 3285–3292.
(28) Nam, K. W.; Wang, X. J.; Yoon, W. S.; Li, H.; Huang, X. J.; Haas, O.; Bai, J. M.; Yang, X. Q. *Electrochem. Commun.* **2009**, *11*(4), 913–916.
(29) Zhang, Y.; Sun, C. S.; Zhou, Z. *Electrochem. Commun.* **2009**, *11*(6), 1183–1186.
(30) Kobayashi, G.; Yamada, A.; Nishimura, S.; Kanno, R.; Kobayashi, Y.; Seki, S.; Ohno, Y.; Miyashiro, H. *J. Power Sources* **2009**, *189*, 397–401.
(31) Wang, G. X.; Bewlay, S.; Yao, J.; Ahn, J. H.; Dou, S. X.; Liu, H. K. *Electrochem. Solid State Lett.* **2004**, *7*(12), A503–A506.
(32) Yamada, A.; Kudo, Y.; Liu, K. Y. *J. Electrochem. Soc.* **2001**, *148* (10), A1153–A1158.
(33) Yamada, A.; Hosoya, M.; Chung, S.-C.; Kudo, Y.; Hinokuma, K.; Liu, K.-Y.; Nishi, Y. *J. Power Sources* **2003**, *119*−*121*, 232–238.
(34) Perdew, J. P.; Burke, K.; Ernzerhof, M. *Phys. Rev. Lett.* **1996**, *77* (18), 3865–3868.
(35) Kresse, G.; Furthmuller, J. *Comput. Mater. Sci.* **1996**, *6*(1), 15–50.
(36) Kang, K.; Chen, C. H.; Hwang, B. J.; Ceder, G. *Chem. Mater.* **2004**, *16*(13), 2685–2690.
(37) Zhou, F.; Cococcioni, M.; Marianetti, C. A.; Morgan, D.; Ceder, G. *Phys. Rev. B* **2004**, *70*(23), 8.
(38) Zhou, F.; Kang, K. S.; Maxisch, T.; Ceder, G.; Morgan, D. *Solid State Commun.* **2004**, *132*(3−4), 181–186.
(39) Breger, J.; Meng, Y. S.; Hinuma, Y.; Kumar, S.; Kang, K.; Shao-Horn, Y.; Ceder, G.; Grey, C. P. *Chem. Mater.* **2006**, *18* (20), 4768–4781.
(40) Kang, K.; Morgan, D.; Ceder, G. Phys. Rev. B **2009**, *79*, (1).
(41) Anisimov, V. I.; Zaanen, J.; Andersen, O. K. *Phys. Rev. B* **1991**, *44* (3), 943.
(42) Anisimov, V. I.; Aryasetiawan, F.; Lichtenstein, A. I. *J. Phys. Condens. Matter* **1997**, *9*(4), 767–808.
(43) Jonsson, H.; Mills, G.; Jacobsen, K. W.; Berne, B. J., In *Classical and Quantum Dynamics in Condensed Phase Simulations*; Chandler, D., Berne, B. J., Ciccotti, G., Coker, D. F., Eds.; World Scientific: Singapore, 1998; p 385.
(44) Morgan, D.; Van der Ven, A.; Ceder, G. *Electrochem. Solid State Lett.* **2004**, *7*(2), A30–A32.

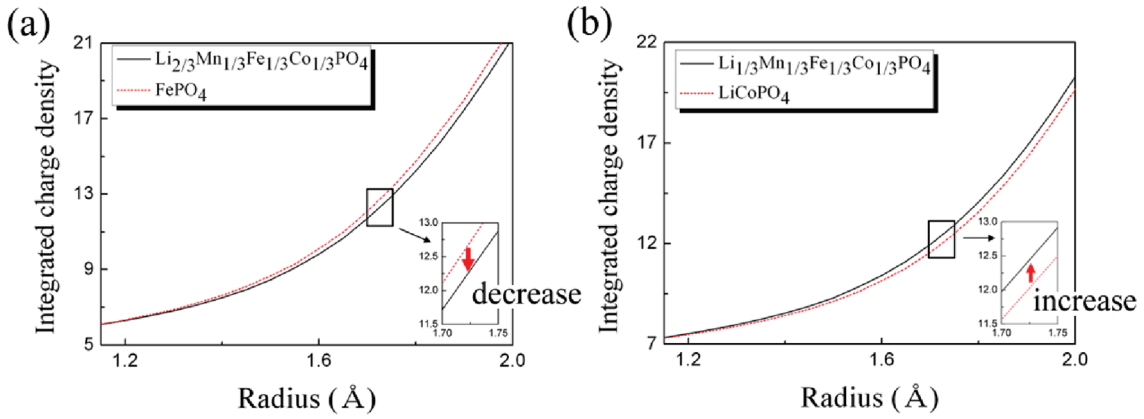

Figure 2. Integrated charge density as a function of the integration radius of transition metal ions: (a) Fe^{3+} and (b) Co^{2+}. Solid lines are used for $Li_xMn_{1/3}Fe_{1/3}Co_{1/3}PO_4$ and dashed lines are used for Li_xMPO_4.

Mn^{3+}/Mn^{2+}, eight Li are fixed and one Li is allowed to diffuse in the unit cell of $Li_{9/24}Mn_{1/3}Fe_{1/3}Co_{1/3}PO_4$ and $Li_{9/24}MnPO_4$. The nudged elastic band method is used with seven replicas of the system, which are initiated by linear interpolation between the initial and final states of the path.[45] All lattice parameters are fixed, but all the internal degrees of freedom are relaxed.

3. Results and Discussion

3.1. Local Structure Evolution and Electronic Structure. First, we investigated the redox reaction of $Li_xMn_{1/3}Fe_{1/3}Co_{1/3}PO_4$ and its accompanied local structure evolution. The structural parameters, such as bond lengths between transition metal (M = Mn, Fe or Co, hereafter) and oxygen in MO_6 octahedra and volumes of the octahedra, were calculated for $Li_xMn_{1/3}Fe_{1/3}Co_{1/3}PO_4$ at $x = 1$, $x = {}^2/_3$, $x = {}^1/_3$, and $x = 0$ (see Figure 1 and Supporting Information for detailed information). The average volumes of these MO_6 octahedra subsequently change as a result of the corresponding M^{3+}/M^{2+} redox reaction. At the first third of Li deintercalation ($Li_{2/3}Mn_{1/3}Fe_{1/3}Co_{1/3}PO_4$), mainly the volume of FeO_6 decreases, as Fe ions are first oxidized locally. At this composition, volumes of MnO_6 and CoO_6 are also slightly affected even though Mn and Co ions are not oxidized yet. This is because the change of Fe−O bonding also alters nearby Mn−O or Co−O bond length. Similarly, at $Li_{1/3}Mn_{1/3}Fe_{1/3}Co_{1/3}PO_4$, the volume of MnO_6 mainly decreases locally, and those of FeO_6 and CoO_6 also slightly decrease. Even though MO_6 volume generally decreases with delithiation, some bond lengths elongate and others shrink due to the Jahn−Teller distortion of Mn^{3+}. For example, the bond distance of Mn−O3′ noticeably increases from 2.29 to 2.33 Å, while other Mn−O bonds shrink with the oxidation of the Mn ion. Also, one should note that Jahn−Teller distortions are remarkably reduced in $Li_xMn_{1/3}Fe_{1/3}Co_{1/3}PO_4$ (Mn−O3, 2.02; Mn−O3′, 2.33) when compared to Li_xMnPO_4 (Mn−O3, 1.99; Mn−O3′, 2.45). Neighboring FeO_6 and CoO_6 may constrain the asymmetric distortion of MnO_6. Finally, the volume of CoO_6 decreases significantly at the last delithiation step.

Charge density around each transition metal of delithiated $Li_xMn_{1/3}Fe_{1/3}Co_{1/3}PO_4$ is observed to be different from that of the single component Li_xMPO_4. Figure 2 shows the charge density integrated around Fe (Figure 2a) or Co (Figure 2b) for some Li compositions where each transition metal is supposed to be in the same oxidation state for both multicomponent and single-component olivines. The charge density between Fe^{3+} and O ions in $Li_{2/3}Mn^{2+}{}_{1/3}Fe^{3+}{}_{1/3}Co^{2+}{}_{1/3}PO_4$ is noticeably smaller than that in $Fe^{3+}PO_4$, as shown in Figure 2a. This is attributed to the Fe^{3+}−O−M^{2+} (M = Mn, Co) interactions in $Li_xMn_{1/3}Fe_{1/3}Co_{1/3}PO_4$, which cause weaker covalent bonding between Fe and O.[9,46] Similarly, Figure 2b indicates that the charge density between Co^{2+} and O ions in $Li_{1/3}Mn^{3+}{}_{1/3}Fe^{3+}{}_{1/3}Co^{2+}{}_{1/3}PO_4$ is larger than that in $LiCo^{2+}PO_4$. This is also attributed to the Co^{2+}−O−M^{3+} (M = Mn, Fe) interactions, which lead to strong covalent bonding of Co−O. It is apparent that the mixed valency of transition metals affects the charge distribution between oxygen and each transition metal. The change of covalency between M and O is expected to shift the redox potential of each transition metal.[27] Goodenough et al. suggested that the weakened Fe−O covalency as a result of the strong P−O covalency shifts Fe^{3+}/Fe^{2+} redox potential up in $LiFePO_4$;[9] a similar mechanism is likely to affect the Fe^{3+}/Fe^{2+} redox potential in the mixed transition metal.[14,30] On the contrary, the Co^{3+}/Co^{2+} redox potential will become lower in the multicomponent olivine as compared to in the $LiCoPO_4$ due to stronger covalency. The shift of the redox potential will be further discussed below.

3.2. Li Mobility and Electron (Polaron) Conductivity. Small polaron hopping has been suggested to be the main electron conduction mechanism in the olivine.[21,47] Its sluggish kinetics were mainly attributed to the poor electronic conductivity of phosphate systems. A polaron is a quasiparticle formed by an electron and its self-induced distortion. The large lattice distortion induced by Jahn−Teller Mn^{3+} is partly responsible for the low

(45) Curtarolo, S.; Morgan, D.; Ceder, G. *CALPHAD* **2005**, *29*(3), 163–211.
(46) Padhi, A. K.; Nanjundaswamy, K. S.; Masquelier, C.; Goodenough, J. B. *J. Electrochem. Soc.* **1997**, *144*(8), 2581–2586.
(47) Ellis, B.; Perry, L. K.; Ryan, D. H.; Nazar, L. F. *J. Am. Chem. Soc.* **2006**, *128*(35), 11416–11422.

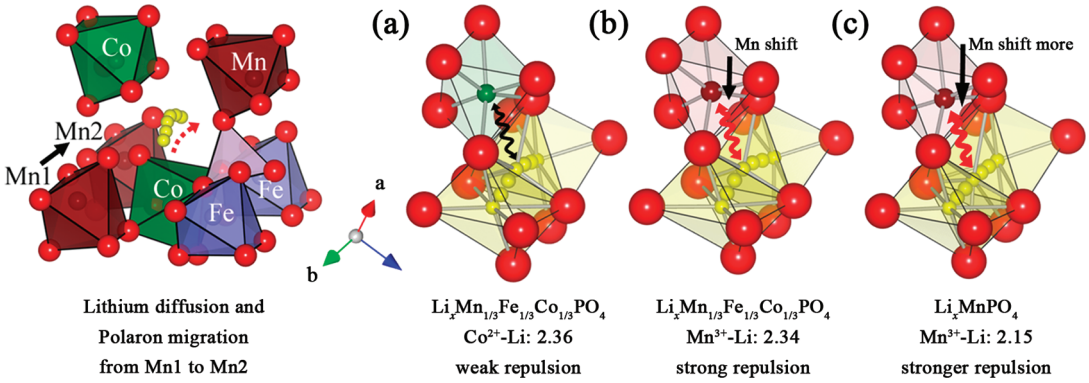

Figure 3. Li−polaron diffusion pathway and interaction between Li and M at transition state: (a) Li and Co in $Li_xMn_{1/3}Fe_{1/3}Co_{1/3}PO_4$, (b) Li and Mn in $Li_xMn_{1/3}Fe_{1/3}Co_{1/3}PO_4$, and (c) Li and Mn in Li_xMnPO_4. The distances between the center of the tetrahedral site of Li and M are shown.

power capability of Li_xMnPO_4 compared to Li_xFePO_4.[15] Our calculations show that the Jahn−Teller effect can be reduced by the substitution of transition metals in $LiMnPO_4$, and small polarons localized around the Mn ion can thus migrate faster. When Li ions and polarons diffuse together due to strong Li−polaron interaction,[48] the calculated activation barrier of the polaron migration is 808.2 meV for Li_xMnPO_4 and 552.7 meV for $Li_xMn_{1/3}Fe_{1/3}Co_{1/3}PO_4$, respectively (see Supporting Information). Since the polaron mobility is inversely proportional to the exponential of the activation barrier, a more than 200 meV difference in the activation barrier will result in a significant difference in the electrochemical activity of Mn in these two olivine systems. It should be also noted that the activation barrier of polaron migration in Li_xMnPO_4 is over 100 meV higher than that of Li_xFePO_4 as reported by Ceder et al., who used the same computational scheme.[21] A simple calculation demonstrates that the diffusivity of the Mn polaron is at least 3 orders of magnitude smaller than that of the Fe polaron. This clearly explains why the rate capability of $LiMnPO_4$ should be lower than that of $LiFePO_4$.

Li diffusion is also strongly affected by the species of the nearest transition metal to a hopping Li. Figure 3a,b show calculated Li hopping processes in the multicomponent olivine, where the Co octahedron (Figure 3a) or the Mn octahedron (Figure 3b) edge-shares with the intermediate site of Li diffusion, respectively. During Li motion, the Li in the initial octahedral site jumps through the intermediate tetrahedral site, which edge-shares with the octahedral transition metal and arrives at the next octahedral site.[4,49] Due to the edge-sharing transition metal, the Li diffusion pathway appears to be sinusoidal. This is in agreement with previous reports.[4,49] One interesting observation can be made when the intermediate site edge-shares with the Mn^{3+} octahedron. As discussed in the previous section, the bond lengths of Mn−O3 noticeably shrink, whereas those of Mn−O3′ elongate due to Jahn−Teller distortion of the Mn octahedron (see Figure 1). These asymmetric distortions cause the Mn ion to shift off the center of the MnO_6 octahedron and to become closer to the Li diffusion pathway. As a consequence, the Li diffusion is strongly restricted by the repulsion from Mn^{3+}, which is not observed for Li hopping near Co or Fe. It should be noted that the negative effect of Jahn−Teller Mn on Li mobility is more severe in $LiMnPO_4$. The shrinkage of Mn−O3 and the elongation of Mn−O3′ are greater in $LiMnPO_4$, as shown in Figure 3c. While the distance between Mn^{3+} and the center of the intermediate Li tetrahedron is 2.357 Å in $Li_xMn_{1/3}Fe_{1/3}Co_{1/3}PO_4$, the distance noticeably reduces to 2.150 Å in Li_xMnPO_4 as a result of the larger asymmetry. The proximity of a Mn^{3+} ion to a Li diffusion pathway will significantly increase the activation barrier for Li motion. This strongly implies that the kinetics of Mn-based olivine electrode can be improved by reducing the Jahn−Teller effect and modifying the environment of Li diffusion pathway through the substitution of multiple transition metals in the structure.

3.3. One-Phase Li Insertion/Extraction Processs. Olivine cathodes such as $LiMnPO_4$, $LiFePO_4$, and $LiCoPO_4$ typically operate by a two-phase Li insertion/extraction process at room temperature in an electrochemical Li cell.[9,50−53] Zhou et al. reported that the effectively attractive M^{2+}−Li^+ (or M^{3+}−vacancy) interaction is the main contributer to the phase separation of the olivine cathode with delithiation.[51,54] In spite of the repulsions of Li^+−Li^+ and e^-−e^-, Li ions tend to be brought together in Li_xFePO_4 due to the strong attraction of Fe^{2+}−Li^+, resulting in a phase separation. On the other hand, Yamada et al. reported a single-phase region in a mixed cation system such as $Li_x(Fe_{1-y}Mn_y)PO_4$ at a particular x region.[32] It was speculated by Malilk et al. that the strong attraction of Mn^{2+}−Li^+ is disturbed by the simultaneous Fe^{3+}−Li^+ repulsion due to the random coexistence of

(48) Maxisch, T.; Ceder, G. *Phys. Rev. B* **2006**, *73*(17), 4.
(49) Islam, M. S.; Driscoll, D. J.; Fisher, C. A. J.; Slater, P. R. *Chem. Mater.* **2005**, *17*(20), 5085–5092.
(50) Chen, G. Y.; Song, X. Y.; Richardson, T. J. *Electrochem. Solid State Lett.* **2006**, *9*(6), A295–A298.
(51) Zhou, F.; Maxisch, T.; Ceder, G. *Phys. Rev. Lett.* **2006**, *97*(15), 4.
(52) Delmas, C.; Maccario, M.; Croguennec, L.; Le Cras, F.; Weill, F. *Nat. Mater.* **2008**, *7*(8), 665–671.
(53) Laffont, L.; Delacourt, C.; Gibot, P.; Wu, M. Y.; Kooyman, P.; Masquelier, C.; Tarascon, J. M. *Chem. Mater.* **2006**, *18*(23), 5520–5529.
(54) Zhou, F.; Marianetti, C. A.; Cococcioni, M.; Morgan, D.; Ceder, G. *Phys. Rev. B* **2004**, *69*(20), 4.

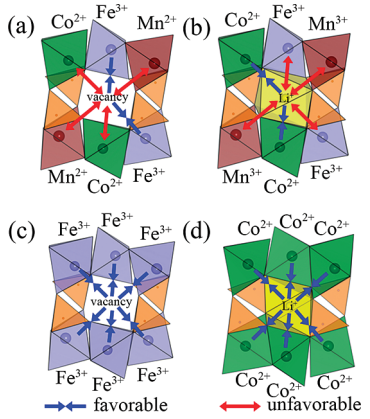

Figure 4. The arrangements of neighbor transition metals around vacancy/Li ion in $Li_xMn_{1/3}Fe_{1/3}Co_{1/3}PO_4$ and Li_xMPO_4 (M = Fe, Co): (a) vacancy in $Li_{2/3}Mn_{1/3}Fe_{1/3}Co_{1/3}PO_4$, (b) Li in $Li_{1/3}Mn_{1/3}Fe_{1/3}Co_{1/3}PO_4$, (c) vacancy in $FePO_4$, and (d) Li in $LiCoPO_4$. Arrows are used to indicate the favorable and unfavorable interactions between transition metal and Li or vacancy.

Mn^{2+} and Fe^{3+} in the structure, thereby decreasing the driving force for the phase separation.[20] In our multicomponent $Li_xMn_{1/3}Fe_{1/3}Co_{1/3}PO_4$, Li ions are also often surrounded simultaneously by M^{2+} and M^{3+} during charging/discharging (Figure 4) because transition metal ions are homogeneously mixed and their redox potentials are distinct. For example, at $Li_{2/3}Mn_{1/3}Fe_{1/3}Co_{1/3}PO_4$, where Fe is +3 and both Mn and Co are +2, some Li ions will have Mn^{2+} and Co^{2+} as neighbors, whereas others will have Fe^{3+} as neighbors. Li ions (effectively hole) near Mn^{2+} and Co^{2+} are energetically favored due to the strong attraction of $M^{2+}-Li^+$, whereas those near Fe^{3+} are not favored because of the repulsion of $Fe^{3+}-Li^+$.[51] Li ions will be brought together near Mn and Co ions, while vacancies will be preferred near Fe^{3+}. If Fe ions are well distributed all over, the strong tendency toward vacancy (V) around Fe^{3+} will result in a solid solution-like phase rather than the segregation of a vacancy-rich delithiated phase at this composition. Similarly, at $Li_{1/3}Mn_{1/3}Fe_{1/3}Co_{1/3}PO_4$, where Fe and Mn are +3 and Co is +2, Li ions tend to be brought together near Co^{2+}. Li will have a strong tendency to be uniformly distributed when Co^{2+} is well mixed throughout. Therefore, the driving force for the phase separation between lithiated and delithiated phases decreases when multielements are uniformly substituted in the structure. This agrees well with the recent experimental evidence that Li de/intercalation occurs via a one-phase reaction in $Li_xMn_{1/3}Fe_{1/3}Co_{1/3}PO_4$ throughout the $0 \le x \le 1$ range.[27]

3.4. Shift of Equilibrium Potential. The shift of equilibrium potential in mixed cation systems such as $LiMn_{1-y}Fe_yPO_4$ was reported by Kobayashi et al.[30] and Malik et al.[20] An upshift of the Fe^{3+}/Fe^{2+} redox potential and a down-shift of the Mn^{3+}/Mn^{2+} redox potential of about 0.1−0.3 V were observed experimentally and computationally.[20,30] Kobayashi et al. explained these phenomena by the change of ionic character of the transition metal and showed that the redox potential can be tuned by controlling the covalent mixing of M−O.[30] Changes of covalency in the bonding of $Fe^{3+}-O$ and $Co^{2+}-O$ in $Li_xMn_{1/3}Fe_{1/3}Co_{1/3}PO_4$ were also observed in our calculations, as described earlier. Charge density between the transition metal and neighboring oxygen changes with the effect of mixed transition metal ions, which will make covalent bonding either weaker or stronger. Weaker covalent (strong ionic) bonding of $Fe^{3+}-O$ increases the potential of the Fe^{3+}/Fe^{2+} redox couple and stronger covalent (weaker ionic) bonding of $Co^{2+}-O$ decreases the potential of the Co^{3+}/Co^{2+} redox couple.

Recently, the shift of potential was also understood with respect to the change in the relative energy of the intermediate compounds. In their first-principles study, Malik et al. claimed that the unfavorable Li^+-Fe^{3+} interaction leads to the increased energy of the intermediate state, which decreases the potential of the Mn^{3+}/Mn^{2+} redox couple and increases the potential of the Fe^{3+}/Fe^{2+} redox couple. In our case, the energetic states of intermediate compositions such as $Li_{2/3}Mn_{1/3}Fe_{1/3}Co_{1/3}PO_4$ and $Li_{1/3}Mn_{1/3}Fe_{1/3}Co_{1/3}PO_4$ also contributed to the shift of potential. During charging, Fe ions are first oxidized, becoming Fe^{3+} in $Li_{2/3}Mn_{1/3}Fe_{1/3}Co_{1/3}PO_4$. Fe^{3+} attracts vacancy due to the strong interaction between Fe^{3+} and V. However, some vacancies attracted to the Fe^{3+} ion are also surrounded by Mn^{2+} and Co^{2+} which have not yet been oxidized, as shown in Figure 4a. The unfavorable $Mn^{2+}-V$ and $Co^{2+}-V$ interactions will increase the energy of this intermediate composition, $Li_{2/3}Mn_{1/3}Fe_{1/3}Co_{1/3}PO_4$. This is in contrast to Li_xFePO_4, where vacancies are surrounded mostly by +3 ions (Fe^{3+}), as shown in Figure 4c. The higher energy of the intermediate composition will result in higher voltage in this region where Fe^{3+}/Fe^{2+} redox reaction occurs. Similarly, Co ions are the last to be oxidized in the delithiation process and remain +2 in $Li_{1/3}Mn_{1/3}Fe_{1/3}Co_{1/3}PO_4$, whereas Fe and Mn ions have already become +3. Co^{2+} attracts the Li ion in $Li_{1/3}Mn_{1/3}Fe_{1/3}Co_{1/3}PO_4$ due to the attractive interaction of $Co^{2+}-Li^+$. Some Li ions near Co^{2+} are also surrounded by Fe^{3+} and Mn^{3+} at this composition, as shown in Figure 4b. The unfavorable $Fe^{3+}-Li^+$ and $Mn^{3+}-Li^+$ interactions will increase the energy of $Li_{1/3}Mn_{1/3}Fe_{1/3}Co_{1/3}PO_4$ and therefore decrease the voltage in this range where the Co^{3+}/Co^{2+} redox reaction occurs. This is in contrast to Li_xCoPO_4, where Li ions are surrounded mostly by +2 ions (Co^{2+}), as shown in Figure 4d. Change in the Mn^{3+}/Mn^{2+} redox couple is negligible, since the energies of both intermediate compositions increase simultaneously by almost the same amount. It should be noted that the shifts of redox potentials for both Fe and Co are rather beneficial for a practical purpose. The higher energy density is achieved through the increased Fe^{3+}/Fe^{2+}, while the decreased Co^{3+}/Co^{2+} redox potential ensures the Co activity in a reasonable voltage range. This points out that the multicomponent olivine can be an effective strategy for tailoring the electrochemical properties of olivine cathodes.

4. Conclusions

The in-depth study of the multicomponent effect on the structural and electrochemical properties of olivine

cathodes was conducted using first-principles calculations. The distribution of multiple transition metals in olivine structure alters local structure and electronic structure, affecting its kinetic and thermodynamic properties. Local structure changes, such as the Jahn−Teller effect of Mn, could be reduced, therefore, improving Li mobility and electron (polaron) conductivity. Li insertion/extraction occurs through a one-phase reaction due to multiple interactions of M/Li or M/vacancy. The redox potential also could shift as a result of charge redistribution and the relative energy change from the multiple M/Li interactions. All of these observations clearly point toward the conclusioin that multicomponent olivine can be a useful system for tailoring the electrochemical properties of olivine compounds for designing better-performing Li rechargeable batteries.

Acknowledgment. This research was supported by General Research Grant program through the Korea Science and Engineering Foundation funded by the Ministry of Education, Science and Technology (R01-2008-000-10913-0), the Korea Research Foundation Grant funded by the Korean Government (MEST) (KRF-2008-331-D00243), the Korea Science & Engineering Foundation (KOSEF) grant (WCU program, 31-2008-000-10055-0) funded by the Ministry of Education and Science & Technology (MEST), and the Korea Science and Engineering Foundation (KOSEF) grant funded by the Korea government (MEST) (R11-2008-058-01003-0). This work was also supported by Energy Resources Technology R&D program (20092020100040) under the Ministry of Knowledge Economy, Republic of Korea. This work was also supported by Grant No. KSC-2009-S03-0011 from Korea Institute of Science and Technology Information.

Supporting Information Available: Table of the calculated structure parameters and figure of the calculated activation barrier of polaron migration (PDF). This material is available free of charge via the Internet at http://pubs.acs.org.